Optics Letters

Tunable VUV frequency comb for ^{229m}Th nuclear spectroscopy

Chuankun Zhang,[1,*] Peng Li,[2] Jie Jiang,[2] Lars von der Wense,[1] John F. Doyle,[1] Martin E. Fermann,[2] and Jun Ye[1]

[1]JILA, National Institute of Standards and Technology and Department of Physics, University of Colorado, Boulder, Colorado, 80309, USA
[2]IMRA America, Inc., 1044 Woodridge Ave., Ann Arbor, MI 48105, USA
*Corresponding author: chuankun.zhang@colorado.edu

Received 16 August 2022; revised 28 September 2022; accepted 10 October 2022; posted 10 October 2022; published 21 October 2022

Laser spectroscopy of the ^{229m}Th nuclear clock transition is necessary for the future construction of a nuclear-based optical clock. Precision laser sources with broad spectral coverage in the vacuum ultraviolet are needed for this task. Here, we present a tunable vacuum-ultraviolet frequency comb based on cavity-enhanced seventh-harmonic generation. Its tunable spectrum covers the current uncertainty range of the ^{229m}Th nuclear clock transition. © 2022 Optica Publishing Group

https://doi.org/10.1364/OL.473006

Transitions between metastable nuclear states (isomeric transitions), typically in the x ray or γ-ray energy range, have been studied extensively with Mössbauer spectroscopy [1]. Recently, quantum control of nuclear excitation [2,3] has been demonstrated using suitably shaped x ray pulses. However, high-resolution spectroscopy, and specifically the construction of a nuclear-based optical clock, remains an open challenge, mainly due to the lack of narrow-linewidth lasers in the x ray energy range. Among all known nuclear isomeric transitions, ^{229m}Th has a uniquely low excitation energy, suitable for the construction of a nuclear clock. Recent reviews on this topic can be found in Refs. [4–6]. The ^{229m}Th transition energy has been measured to be 8.28 ± 0.17 eV using electron spectroscopy [7] and 8.10 ± 0.17 eV using γ-ray spectroscopy [8]. Very recently, an experiment observing the direct radiative decay of ^{229m}Th narrowed down the nuclear transition energy to 8.338 ± 0.24 eV [9]. The transition energy corresponds to a wavelength of approximately 150 nm in the vacuum-ultraviolet (VUV) spectral region, where table-top narrow-linewidth laser sources are available [10,11].

The ^{229m}Th nuclear transition is expected to have a long radiative lifetime of the order of 10^3 s to 10^4 s [12,13]. This long lifetime corresponds to potentially a high quality factor $Q \approx 10^{20}$, orders of magnitude higher than that in state-of-the-art atomic clocks [14]. Furthermore, due to the small nuclear electromagnetic moments and shielding effects from the electrons, the ^{229m}Th transition is expected to be insensitive to external perturbations. The high quality factor and high resistance to external perturbation make ^{229m}Th a promising candidate for constructing a nuclear optical clock [15,16]. By applying precision laser measurement tools and coherent quantum control in nuclear physics, a nuclear clock would provide a wide range of new opportunities, including probing the interaction between the electronic shell and the nucleus (e.g., electron bridge effect) [17–20], precise timekeeping with solid-state optical clocks [21–23], and ultrasensitive tests of fundamental physics [24–26].

To develop such a nuclear clock, high-resolution laser spectroscopy of the ^{229m}Th state has to be performed first. There is currently a worldwide effort toward laser spectroscopy of the ^{229m}Th transition employing different laser systems. Nanosecond VUV laser pulses generated via resonant-enhanced four-wave mixing processes reported in Refs. [5,27,28] are currently being used for the ^{229m}Th spectroscopy. The pulsed VUV laser systems offer broadband tuning ranges and are suitable for the initial transition search. Full repetition rate frequency combs in the VUV can be generated using femtosecond enhancement cavities [11,29,30]. Such VUV frequency comb systems are either being used [5,31,32] or being developed [5] for ^{229m}Th spectroscopy.

We propose to perform direct VUV frequency comb spectroscopy [33] of the ^{229m}Th state using the seventh harmonic of an Yb-fiber frequency comb [23]. The discrete frequency comb lines in the VUV can be scanned in parallel to cover the entire comb spectrum [33]. By performing multiple scans with different comb repetition rates and solving for the integer comb mode numbers, one can also directly read out the transition frequency without needing a spectrometer [33]. Once the transition is found, a nuclear clock can be directly constructed by stabilizing the comb to the nuclear transition. A remaining challenge is that the typical bandwidth of a VUV comb is smaller than the uncertainty range of the ^{229m}Th transition [4,11]. Here we present a tunable VUV frequency comb based on a tunable Yb-fiber frequency comb system to mitigate this problem.

The tunable Yb-fiber comb layout is shown in Fig. 1(a). We implemented a low-noise 75 MHz Yb-fiber oscillator [34] and amplified its output in cascaded linear (PM-YSF) and nonlinear (PLMA-YDF-25/250) similariton [35] amplifiers. The output of the nonlinear amplifier gave us a coherent broadband frequency comb for seeding the final-stage high-power fiber amplifier. A fraction (10%) of the nonlinear amplifier output was sent to a highly nonlinear photonic crystal fiber (HNL PCF) for supercontinuum generation. We stabilized the comb carrier-envelope

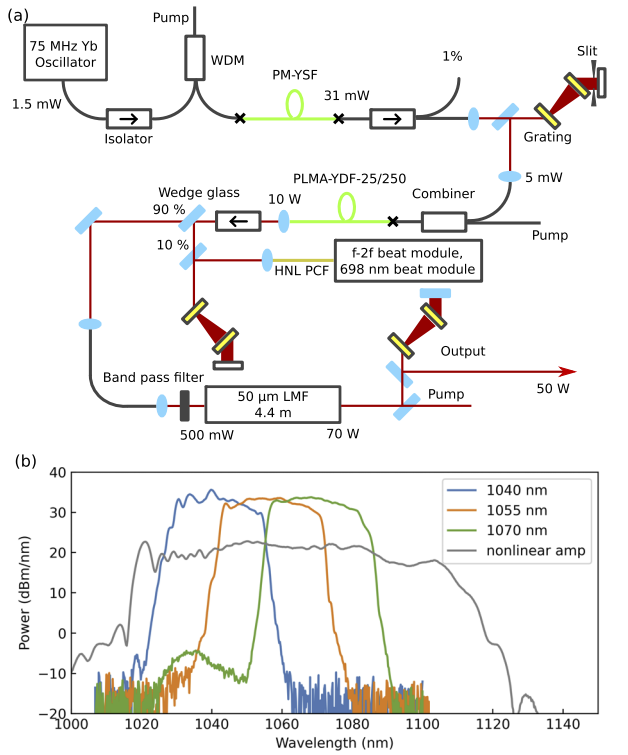

Fig. 1. (a) Tunable Yb-fiber frequency comb. Black lines represent passive fibers; green lines represent active fiber amplifiers; red lines are free-space laser paths. Grating pairs (yellow) are used for temporal compression of the laser pulses. A slit is used in combination with the first grating pair to clean up the spectral output from the oscillator. WDM, wavelength-division multiplexer; PM-YSF, polarization-maintaining Yb-doped single-clad fiber; PLMA-YDF-25/250, polarization-maintaining large-mode-area Yb-doped double-clad fiber with 25/250 µm core/cladding diameter; HNL PCF, highly nonlinear photonic-crystal fiber; LMF, large-mode-area fiber module with 50 µm core diameter. (b) Spectra of the nonlinear similariton amplifier and LMF amplifier output at different wavelength settings.

offset frequency f_{ceo} by the f-2f self-referencing scheme. To fully stabilize the frequency comb structure, we also phase locked one of the comb lines in the supercontinuum to the Sr clock laser at 698 nm [36]. The comb lines can thus be scanned simply by shifting the offset frequency between one comb line and the Sr clock laser [33]. To achieve the desired spectral tunability of the comb, we selected a part of the spectrum from the nonlinear amplifier output using an interference bandpass filter. We can tune the central wavelength continuously from 1040 nm to 1070 nm by changing the angle of the bandpass filter. The filtered light was amplified further in a large-mode-area fiber (LMF) power amplifier. The optical spectra of the nonlinear amplifier and the power amplifier at several different wavelength settings are shown in Fig. 1(b). The spectral filtering and subsequent amplification allowed us to mitigate nonlinear self-phase-modulation in the LMF fiber and obtain high output spectral power. After the final grating compressor, we produced an infrared frequency comb with >50 W average power and <150 fs pulse duration.

The output of this high-power infrared frequency comb was then coherently coupled into a femtosecond enhancement cavity for seventh harmonic generation [11], see Fig. 2(a). This cavity

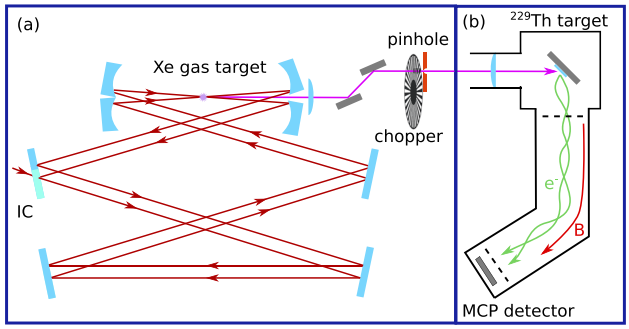

Fig. 2. VUV generation and spectroscopy setup. (a) VUV generation chamber. A detailed description of the noncollinear cavity is presented in Ref. [32]; IC, input coupler. (b) Illustration of spectroscopy setup using a solid-state ^{229}Th target. The green traces (e^-) illustrate the electron trajectory guided by a curved magnetic field (B, red trace); MCP, microchannel plate.

provides an enhancement factor of approximately 100 for the comb peak and average power, necessary for driving the seventh harmonic generation at the original comb repetition rate. We use a noncollinear geometry [32] to extract the generated harmonics efficiently.

While the noncollinear geometry offers high outcoupling efficiency for high-order harmonics, we estimate the extraction efficiency of the seventh harmonic to be only approximately 30% based on numerical simulations [32]. As we only need the seventh harmonic for the nuclear spectroscopy, alternative outcoupling methods [11,37] should be considered. A standard method for cavity-enhanced high harmonic outcoupling is using an intra-cavity plate at the Brewster's angle (Brewster plate) for the fundamental light. Conventional Brewster plate materials such as MgO offer up to 2% coupling efficiency for the seventh harmonic, which is rather low [11,38]. Using nanogratings etched on top of a high reflector, 3% of the seventh harmonic can get diffracted out [39]. Thin plates with high-reflection coatings for the VUV light have been demonstrated before, offering up to 75% reflectivity [40]. However, in long-term operation, they suffer from degradation caused by UV irradiation. A thin plate with antireflection coatings for s-polarized fundamental light at a grazing incidence angle (grazing incidence plate, GIP) was also proposed for extreme-ultraviolet (XUV)-outcoupling [41]. Using 70° incidence angle, a coupling efficiency of 40% is feasible. This technique was recently tested inside an active oscillator cavity [42]. However, fabricating a low-loss GIP for a passive enhancement cavity is challenging. Other outcoupling schemes, such as using mirrors with wedged top layer [43], pierced mirrors [44], or quasi-imaging cavity modes [45] are typically optimized for higher harmonic orders and give relatively low efficiency for the seventh harmonic.

Table 1 summarizes different outcoupling methods discussed above for the intra-cavity generated seventh harmonic.

Table 1. Outcoupling Methods for Seventh Harmonic

Methods	Efficiency	Challenge
Noncollinear	30%	Alignment complexity
Brewster plate	2%	Low efficiency
XUV grating	3%	Low efficiency
XUV HR plate	75%	Degradation
GIP	40%	Loss in intracavity IR

In the detection system, shown in Fig. 2(b), a thin 10 nm film of thorium oxide coating on a platinum-coated Si wafer will be used as the target for the spectroscopy. In the internal-conversion decay process, the excited nuclear state decays dominantly by transferring its energy to an electron instead of emitting a photon. The nuclear transition linewidth is thus broadened by this additional decay channel to approximately 16 kHz [46]. Using the solid-state target allows us to irradiate 10^{13} nuclei in parallel. We plan to perform fast and low-noise detection of the nuclear isomeric decay events by observing the internal-conversion electrons emitted from the surface using a microchannel plate detector.

As described in Ref. [23], we plan to use gated pulses to excite the nuclear transition and synchronously detect the isomeric decay events after the laser is turned off. This detection scheme requires a short laser turnoff time compared with the isomeric lifetime of 10 µs. However, the intracavity Xe plasma generated by the laser causes a VUV fluorescent afterglow lasting tens of µs [47], which would potentially lead to an increased background for the spectroscopy measurement. We thus focused the VUV laser through a 100 µm diameter copper pinhole and implemented an in-vacuum chopper wheel running at 30 000 revolutions per minute to gate the laser. The chopper wheel system allowed us to achieve clean laser gating with sub-microsecond on–off times. Furthermore, we used a magnetic field to guide the electrons to avoid a direct line-of-sight between the target and the microchannel plate detector, see Fig. 2(b). Using this detection system, we reduced the laser-induced background in the nuclear spectroscopy to a negligible amount compared with the background from intrinsic target radioactivity, which is the main source of background.

To drive the $^{229\,m}$Th nuclear transition efficiently, the VUV frequency comb linewidth should be comparable to, or narrower than, the transition linewidth. We quantify the laser linewidth by integrating the phase noise starting from a 1 MHz Fourier frequency [48]. It has been experimentally verified that in the cavity-enhanced harmonic generation processes, just as in other noise-free harmonic generation processes, the phase noise power spectral density (PSD) scales as $S_\phi(f) \propto q^2$, where q is the harmonic order [49]. In our case for the seventh harmonic generation, this scaling poses a 49 times more stringent requirement of the phase noise PSD on the fundamental comb.

To characterize the comb linewidth, we measured the in-loop phase noise of the Yb-fiber comb when stabilized to a 1064 nm low-noise reference laser, which is in turn locked to the JILA Sr clock local oscillator [36]. The comb f_{ceo} is simultaneously stabilized to a radio frequency reference. In addition to the power enhancement, the optical cavity also filters the high-frequency optical phase noise due to its narrow resonance linewidth. Using the phase noise scaling relation and a cavity finesse of 400, we can scale the optical phase noise of the fundamental comb to the phase noise of the seventh harmonic comb, shown in Fig. 3. The integrated phase noise down to 10 Hz is only 0.15 rad in the seventh harmonic. This corresponds to >97% optical power remaining in the coherent VUV frequency comb teeth of 10 Hz linewidth. Additional phase noise on the seventh harmonic from intensity noise via the intensity-dependent dipole phase is negligible [49]. We estimate that the linewidth of our seventh harmonic would be limited to kHz level due to optical path length fluctuations in our experiment setup, which is still narrow compared with the internal-conversion broadened nuclear transition linewidth of 16 kHz.

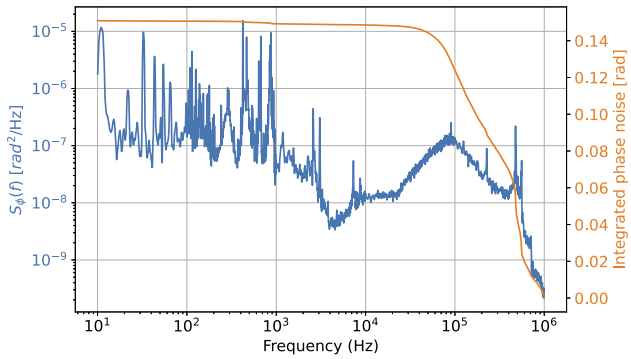

Fig. 3. Phase noise performance of the VUV comb. A low-pass filtering function (corner frequency, 93.75 kHz) corresponding to the transfer function of our enhancement cavity has been applied, which reduces the high-frequency phase noise. The left-hand axis is for phase noise power spectral density (blue curve), and the right-hand axis is for the integrated phase noise (orange curve) integrated from 1 MHz down to the corresponding value of the x axis.

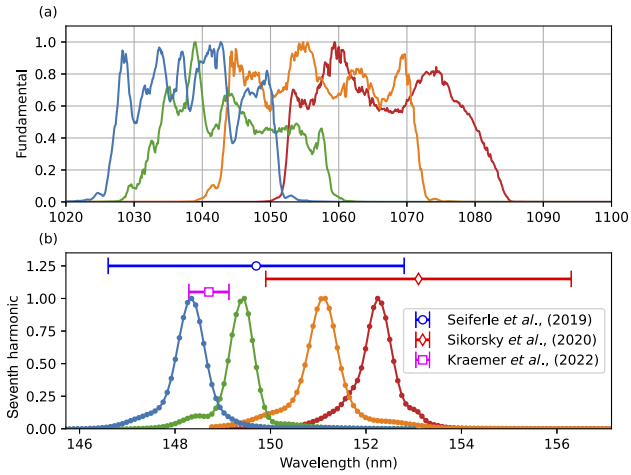

Fig. 4. Comb tunability. (a) Fundamental comb spectrum, measured as the leakage transmission from one of the enhancement cavity mirrors. (b) VUV spectrum of the outcoupled harmonics, measured with a grating-based VUV spectrometer. Horizontal error bars indicate the $^{229\,m}$Th transition uncertainty ($1-\sigma$) ranges given in Seiferle *et al.* [7], Sikorsky *et al.* [8], and Kraemer *et al.* [9]. We obtain similar overall VUV powers at each wavelength setting. Vertical scales in the plots are normalized to unity.

We show several measured fundamental Yb-fiber comb spectra in Fig. 4(a) under different wavelength settings. The corresponding VUV frequency comb spectra, measured using a grating-based spectrometer (HP Spectroscopy, easyLIGHT) with <0.1 nm resolution, are shown in Fig. 4(b). We estimate the VUV power per comb line to be approximately 1 nW delivered onto the target, sufficient for the nuclear transition search [23]. The tunable comb was initially designed to cover the energy range given in Ref. [7] before the publication of Ref. [8]. A very recent measurement [9] of the nuclear transition energy indicates that we can indeed cover the nuclear transition wavelength with our VUV comb. We note that using a longer fiber in the final stage amplifier can potentially shift the spectral coverage to longer wavelengths for other applications.

In conclusion, we have constructed a tunable VUV frequency comb dedicated to our ^{229m}Th nuclear spectroscopy. The tuning implemented in the Yb-fiber comb amplifier system allows us to easily tune the VUV spectrum to cover the ^{229m}Th nuclear transition uncertainty range. Furthermore, once the clock transition is found, the VUV comb structure can serve directly as the clockwork for reading out the transition frequency and constructing a solid-state nuclear clock referenced to our existing Sr optical atomic clock.

Funding. Army Research Office (W911NF2010182); Air Force Office of Scientific Research (FA9550-19-1-0148); National Science Foundation (PHY-1734006); National Institute of Standards and Technology.

Acknowledgments. We thank J. Weitenberg, A. Ozawa, O. Pronin, A. L. Gaeta, Y. Okawachi, P. St. J. Russell, F. Tani, J. Lampen, J. S. Higgins, and L. R. Liu for helpful discussions. Lars v. d. Wense acknowledges support from the Alexander von Humboldt Foundation.

Disclosures. The authors declare no conflicts of interest.

Data availability. Data underlying the results presented in this paper are not publicly available at this time but may be obtained from the authors upon reasonable request.

REFERENCES

1. N. N. Greenwood, *Mössbauer Spectroscopy* (Springer Science & Business Media, 2012).
2. T. J. Bürvenich, J. Evers, and C. H. Keitel, Phys. Rev. Lett. **96**, 142501 (2006).
3. K. P. Heeg, A. Kaldun, C. Strohm, C. Ott, R. Subramanian, D. Lentrodt, J. Haber, H.-C. Wille, S. Goerttler, R. Rüffer, C. H. Keitel, R. Röhlsberger, T. Pfeifer, and J. Evers, Nature **590**, 401 (2021).
4. L. von der Wense and B. Seiferle, Eur. Phys. J. A **56**, 277 (2020).
5. E. Peik, T. Schumm, M. Safronova, A. Palffy, J. Weitenberg, and P. G. Thirolf, Quantum Sci. Technol. **6**, 034002 (2021).
6. K. Beeks, T. Sikorsky, T. Schumm, J. Thielking, M. V. Okhapkin, and E. Peik, Nat. Rev. Phys. **3**, 238 (2021).
7. B. Seiferle, L. von der Wense, P. V. Bilous, I. Amersdorffer, C. Lemell, F. Libisch, S. Stellmer, T. Schumm, C. E. Düllmann, A. Pálffy, and P. G. Thirolf, Nature **573**, 243 (2019).
8. T. Sikorsky, J. Geist, D. Hengstler, S. Kempf, L. Gastaldo, C. Enss, C. Mokry, J. Runke, C. E. Düllmann, P. Wobrauschek, K. Beeks, V. Rosecker, J. H. Sterba, G. Kazakov, T. Schumm, and A. Fleischmann, Phys. Rev. Lett. **125**, 142503 (2020).
9. S. Kraemer, J. Moens, and M. Athanasakis-Kaklamanakis, *et al.*, "Observation of the radiative decay of the 229Th nuclear clock isomer," arXiv:2209.10276v1 (2022).
10. W. Ubachs, K. Eikema, W. Hogervorst, and P. Cacciani, J. Opt. Soc. Am. B **14**, 2469 (1997).
11. I. Pupeza, C. Zhang, M. Högner, and J. Ye, Nat. Photonics **15**, 175 (2021).
12. E. Tkalya, C. Schneider, J. Jeet, and E. R. Hudson, Phys. Rev. C **92**, 054324 (2015).
13. N. Minkov and A. Pálffy, Phys. Rev. Lett. **122**, 162502 (2019).
14. T. Bothwell, C. J. Kennedy, A. Aeppli, D. Kedar, J. M. Robinson, E. Oelker, A. Staron, and J. Ye, Nature **602**, 420 (2022).
15. E. Peik and C. Tamm, Europhys. Lett. **61**, 181 (2003).
16. C. J. Campbell, A. G. Radnaev, A. Kuzmich, V. A. Dzuba, V. V. Flambaum, and A. Derevianko, Phys. Rev. Lett. **108**, 120802 (2012).
17. E. Tkalya, Soviet Journal of Nuclear Physics **55**, 1611 (1992).
18. S. Porsev, V. Flambaum, E. Peik, and C. Tamm, Phys. Rev. Lett. **105**, 182501 (2010).
19. F. Karpeshin and M. Trzhaskovskaya, Phys. Rev. C **95**, 034310 (2017).
20. P. V. Bilous, H. Bekker, J. C. Berengut, B. Seiferle, L. von der Wense, P. G. Thirolf, T. Pfeifer, J. R. C. López-Urrutia, and A. Pálffy, Phys. Rev. Lett. **124**, 192502 (2020).
21. W. G. Rellergert, D. DeMille, R. Greco, M. Hehlen, J. Torgerson, and E. R. Hudson, Phys. Rev. Lett. **104**, 200802 (2010).
22. G. Kazakov, A. Litvinov, V. Romanenko, L. Yatsenko, A. Romanenko, M. Schreitl, G. Winkler, and T. Schumm, New J. Phys. **14**, 083019 (2012).
23. L. von der Wense and C. Zhang, Eur. Phys. J. D **74**, 146 (2020).
24. P. G. Thirolf, B. Seiferle, and L. von der Wense, Ann. Phys. **531**, 1800381 (2019).
25. A. Banerjee, H. Kim, O. Matsedonskyi, G. Perez, and M. S. Safronova, J. High Energy Phys **2020**, 153 (2020).
26. P. Fadeev, J. C. Berengut, and V. V. Flambaum, Phys. Rev. A **102**, 052833 (2020).
27. J. Jeet, "Search for the low lying transition in the ^{229}Th nucleus," Ph.D. thesis, (University of California, Los Angeles, 2018).
28. L. C. von der Wense, B. Seiferle, C. Schneider, J. Jeet, I. Amersdorffer, N. Arlt, F. Zacherl, R. Haas, D. Renisch, P. Mosel, M. Kovacev, U. Morgner, C. E. Düllmann, E. R. Hudson, and P. G. Thirolf, Hyperfine Interact. **240**, 23 (2019).
29. R. J. Jones, K. D. Moll, M. J. Thorpe, and J. Ye, Phys. Rev. Lett. **94**, 193201 (2005).
30. C. Gohle, T. Udem, M. Herrmann, J. Rauschenberger, R. Holzwarth, H. A. Schuessler, F. Krausz, and T. W. Hänsch, Nature **436**, 234 (2005).
31. J. Seres, E. Seres, C. Serrat, E. Young, J. Speck, and T. Schumm, Opt. Express **27**, 6618 (2019).
32. C. Zhang, S. B. Schoun, C. M. Heyl, G. Porat, M. B. Gaarde, and J. Ye, Phys. Rev. Lett. **125**, 093902 (2020).
33. A. Cingöz, D. C. Yost, T. K. Allison, A. Ruehl, M. E. Fermann, I. Hartl, and J. Ye, Nature **482**, 68 (2012).
34. Y. Li, N. Kuse, A. Rolland, Y. Stepanenko, C. Radzewicz, and M. E. Fermann, Opt. Express **25**, 18017 (2017).
35. M. E. Fermann, V. Kruglov, B. Thomsen, J. M. Dudley, and J. D. Harvey, Phys. Rev. Lett. **84**, 6010 (2000).
36. E. Oelker, R. Hutson, C. Kennedy, L. Sonderhouse, T. Bothwell, A. Goban, D. Kedar, C. Sanner, J. Robinson, G. Marti, D. Matei, T. Legero, M. Giunta, R. Holzwarth, F. Riehle, U. Sterr, and J. Ye, Nat. Photonics **13**, 714 (2019).
37. K. D. Moll, R. J. Jones, and J. Ye, Opt. Express **14**, 8189 (2006).
38. E. D. Palik, *Handbook of Optical Constants of Solids*, Vol. 3 (Academic Press, 1998).
39. D. Yost, T. Schibli, and J. Ye, Opt. Lett. **33**, 1099 (2008).
40. A. Ozawa, Z. Zhao, M. Kuwata-Gonokami, and Y. Kobayashi, Opt. Express **23**, 15107 (2015).
41. O. Pronin, V. Pervak, E. Fill, J. Rauschenberger, F. Krausz, and A. Apolonski, Opt. Express **19**, 10232 (2011).
42. J. Fischer, J. Drs, F. Labaye, N. Modsching, M. Müller, V. J. Wittwer, and T. Südmeyer, Opt. Express **30**, 30969 (2022).
43. I. Pupeza, E. E. Fill, and F. Krausz, Opt. Express **19**, 12108 (2011).
44. I. Pupeza, S. Holzberger, T. Eidam, H. Carstens, D. Esser, J. Weitenberg, P. Rußbüldt, J. Rauschenberger, J. Limpert, T. Udem, A. Tünnermann, T. W. Hänsch, A. Apolonski, F. Krausz, and E. Fill, Nat. Photonics **7**, 608 (2013).
45. I. Pupeza, M. Högner, J. Weitenberg, S. Holzberger, D. Esser, T. Eidam, J. Limpert, A. Tünnermann, E. Fill, and V. S. Yakovlev, Phys. Rev. Lett. **112**, 103902 (2014).
46. B. Seiferle, L. Von Der Wense, and P. G. Thirolf, Phys. Rev. Lett. **118**, 042501 (2017).
47. M. Jinno, H. Kurokawa, M. Aono, and H. Ninomiya, Czech. J. Phys. **50**, 433 (2000).
48. J. Hall and M. Zhu, in *International School of Physics Enrico Fermi Course CXVII, Laser Manipulation of Atoms and Ions* (NIST, 1992), pp. 671–701.
49. C. Benko, T. K. Allison, A. Cingöz, L. Hua, F. Labaye, D. C. Yost, and J. Ye, Nat. Photonics **8**, 530 (2014).